Articles

Syntheses, Structures, and Optical Properties of Yellow Ce_2SiS_5, $Ce_6Si_4S_{17}$, and $Ce_4Si_3S_{12}$ Materials

G. Gauthier,† S. Jobic,† M. Evain,† H.-J. Koo,‡ M.-H Whangbo,‡ C. Fouassier,§ and R. Brec*,†

Institut des Matériaux Jean Rouxel, 2 rue de la Houssinière, BP 32229, 44322 Nantes Cedex 3, France, Department of Chemistry, North Carolina State University, Raleigh, North Carolina 27695-8204, and ICMCB, Château de Brivazac, Avenue du Dr Schweitzer, 33608, Pessac Cedex, France

Received March 22, 2002. Revised Manuscript Received September 30, 2002

The Ce−S−Si system has been explored in search of new, yellow nontoxic pigments. We prepared a new Ce−S−Si phase ($Ce_6Si_4S_{17}$), determined the crystal structures of Ce_2SiS_5, $Ce_4Si_3S_{12}$, and $Ce_6Si_4S_{17}$, and measured the chromatic properties of these Ce−S−Si phases. The differences in the yellow hue of these compounds were probed by analyzing their Ce^{3+} ion environments and calculating their electronic band structures. $Ce_6Si_4S_{17}$ is distinguished from Ce_2SiS_5 and $Ce_4Si_3S_{12}$ in terms of the Ce^{3+} structural environment and the Ce^{3+} $4f^1 \rightarrow 5d^0$ transition gap. This gap is wider for $Ce_6Si_4S_{17}$ than for Ce_2SiS_5 and $Ce_4Si_3S_{12}$ (i.e., 2.51 vs. ∼2.36 eV), and $Ce_6Si_4S_{17}$ exhibits room-temperature luminescence whereas Ce_2SiS_5 and $Ce_4Si_3S_{12}$ do not. $Ce_4Si_3S_{12}$ and $Ce_6Si_4S_{17}$ possess chromatic properties similar to those found for industrial pigments such as $PbCrO_4$, $BiVO_4$, and CdS, and show thermal and chemical stabilities.

1. Introduction

There is a strong incentive to develop new colored inorganic materials to substitute for industrial pigments that are based on heavy elements hazardous to health and the environment.[1] As pigments of red to orange hue, sulfides of Ce^{3+} ($4f^15d^0$) ions such as γ-Ce_2S_3 and its alkali-metal derivatives γ-$Ce_{2-x}A_{3x}S_3$ (A = alkali) have been proposed[2−6] and are currently at the stage of industrial production.[7] The chromatic properties of these cerium sulfides arise from the fact that the optical absorption associated with the 4f→5d electronic transition of their Ce^{3+} ions range from ∼1.9 eV to ∼2.1 eV.[8,9] Thus, these compounds appear to be appropriate substitutes for the red and orange cadmium pigments, i.e., the selenium rich $CdSe_{1-x}S_x$ phases used in the plastics industry.[10]

As yellow pigments to substitute for CdS, $PbCrO_4$, and $PbMoO_4$, sulfides of Ce^{3+} ions are also appropriate if their Ce^{3+} $4f^1 \rightarrow 5d^0$ transition starts at ∼2.5 eV. This might be achieved by increasing the net positive charge on the Ce atoms, i.e., by increasing the ionicity of the Ce−S bonds. According to the inductive effect,[11−13] one can increase the ionicity of a Ce−S bond by forming a Ce−S−M bond linkage with a third element M that makes a strong covalent bond with S. An increase in the net positive charge on a cation lowers the energies of its orbitals.[14] In a Ce−S−M compound, one might expect that this energy-lowering effect is larger for the 4f than for the 5d orbitals of Ce, thereby increasing the Ce $4f^1 \rightarrow 5d^0$ gap, because the Ce 4f orbitals are much more localized on the Ce atom than are the Ce 5d orbitals. Indeed, yellow colors are found for cerium thiophosphates (Ce−S−P phases) $CePS_4$,[12] $K_3CeP_2S_8$,[15] $NaCe(P_2)S_6$, and $KCe(P_2)S_6$.[16] Unfortunately, these compounds are not useful pigments because they undergo hydrolysis readily.

* To whom correspondence should be addressed. Phone: +33-2-4037-3917. Fax: +33-2-4037-3995. E-mail: raymond.brec@cnrs-imn.fr.
† Institut des Matériaux Jean Rouxel.
‡ North Carolina State University.
§ ICMCB.

(1) *European Economic Community Guideline*, 9/338/EWG; EEC: Brussels, Belgium, 1991.
(2) Maestro, P. *E. P. Patent* 0203838, April 30, 1985.
(3) Chopin, T.; Guichon, H.; Touret, O. *E. P. Patent* 545746, December 4, 1991.
(4) Macaudière, P. *E. P. Patent* 680930, May 6, 1995.
(5) Maestro, P.; Huguenin, D. *J. Alloys Comp*. **1995**, *225*, 520.
(6) Vasilyeva, I. G.; Ayupov, B. M.; Vlasov, A. A.; Malakhov, V. V.; Macaudière, P.; Maestro, P. *J. Alloys Comp*. **1998**, *268*, 72.
(7) General information can be found from the web site http://www.rhodia-rare-earths.com/gb/materiaux/main/pigments.html.
(8) Zhukov, V.; Mauricot, R.; Gressier, P.; Evain, M. *J. Solid State Chem*. **1997**, *128*, 197.
(9) Perrin, M. A.; Wimmer, E. *Phys. Rev. B* **1996**, *54*, 2428.
(10) *Industrial Inorganic Pigments*; Buxham, G., Ed.; Wiley-VCH: Weinheim, Germany, 1998.
(11) Etourneau, J.; Portier, J.; Ménil, F. *Alloys Met*. **1992**, *188*, 1.
(12) Gauthier, G.; Jobic, S.; Boucher, F.; Macaudière, P.; Huguenin, D.; Rouxel, J. *Chem. Mater*. **1998**, *10*, 2341.
(13) Gauthier, G.; Jobic, S.; Macaudière, P.; Brec, R. *Mater. Res. Soc. Symp*. **1999**, *458*, 667.
(14) Albright, T. A.; Burdett, J. K.; Whangbo, M.-H. *Orbital Interactions in Chemistry*; Wiley: New York, 1985.
(15) Gauthier, G.; Jobic, S.; Brec, R.; Rouxel, J. *Inorg. Chem*. **1998**, *37*, 2332.
(16) Gauthier, G., Thesis, Université de Nantes, 1999.

10.1021/cm0211711 CCC: $25.00
Published on Web 01/22/2003

The electronegativity of Si is not far from that of P, so the inductive effect of Si on the Ce−S bond in a Ce−S−Si linkage would be similar to that of P on the Ce−S bond in a Ce−S−P linkage. Thus, our search for useful yellow pigments was directed to cerium thiosilicates (Ce−S−Si phases). This synthesis effort led us to discover a new Ce−S−Si phase, $Ce_6Si_4S_{17}$. The synthesis of the cerium thiosilicates Ce_2SiS_5[17] and $Ce_4Si_3S_{12}$[18] were already reported, but their crystal structures were not determined. In the present work we determine the crystal structures of $Ce_6Si_4S_{17}$, Ce_2SiS_5, and $Ce_4Si_3S_{12}$ and measure their chromatic properties. Then we discuss how the differences in the optical properties of these Ce−Si−S phases are related to the structural environments of their Ce^{3+} ions by analyzing their local crystal structures and calculating their electronic band structures. Finally, we examine their chemical and thermal stability to evaluate their potential as yellow pigments for industrial uses.

2. Experimental Section

2.1. Sample Preparation. Ce_2SiS_5[17] and $Ce_4Si_3S_{12}$[18] were prepared as reported previously. For each phase, a mixture of γ-Ce_2S_3 (325 mesh, Cerac, 99.9%), Si (Koch-Light Laboratories, 99.99%), and S (Fluka, puriss. > 99.999%) was weighed in the stoichiometric proportions and placed in a silica tube sealed under a primary vacuum (10^{-3} Torr). The blend was heated slowly (4 °C/hr) up to 300 °C, and was then kept at 300 °C for 2 days to allow for the sublimation of S and its subsequent reaction with Si, thus leading to the intermediate SiS_2. Then the temperature was raised slowly (again 4 °C/hr) up to 1050 °C and was maintained at this temperature for 4 days before quenching the silica tubes in air. Samples were ground and then annealed at 700 °C for 7 days with 5% sulfur mass excess to avoid decomposition of the phase and hence ensure the homogeneity of the final product.

Several attempts to prepare pure samples showed the need to use both S and Si in excess. Actually a 10% molar excess of SiS_2 was used with respect to the targeted formula. For example, Ce_2SiS_5 and $Ce_4Si_3S_{12}$ were obtained from the $[Ce_2S_3]/[Si]/[S] = 1.0:1.1:2.2$ and $[Ce_2S_3]/[Si]/[S] = 2.0:3.3:6.6$ starting ratios, respectively. The annealing described above removes the excess SiS_2, which condenses in the cold end of the reaction tube. To eliminate the last traces of SiS_2 and S, samples were washed with ethanol and dried in air.

In the $Ce_2S_3-SiS_2$ system at 1050 °C there exists a third phase, $Ce_6Si_4S_{17}$. The general formulas of the Ce−S−Si phases can be written as $(Ce_2S_3)_m \cdot (SiS_2)_n$, with, $m = n = 1$ for Ce_2SiS_5, $m = 2$ and $n = 3$ for $Ce_4Si_3S_{12}$, and $m = 3$ and $n = 4$ for $Ce_6Si_4S_{17}$. The new phase $Ce_6Si_4S_{17}$ is yellow like Ce_2SiS_5 and $Ce_4Si_3S_{12}$, but shows a yellow/green luminescence at room temperature. The EDXS analysis of the new phase made on single-crystal samples revealed the composition $Ce_6Si_4S_{17}$ and is identical with the structure determination (see below). Pure $Ce_6Si_4S_{17}$ samples can be prepared from the mixture $[Ce_2S_3]/[Si]/[S] = 3.0:4.4:8.8$ under the synthesis conditions used for Ce_2SiS_5 and $Ce_4Si_3S_{12}$. No other phases were detected at the chosen preparative temperature, but it is worth mentioning that a phase with the composition $Ce_6Si_{2+x}S_{14}$ exists and is found to occur at lower temperature.

2.2. Crystal Structure Determination. *Powder Diffraction Study of Ce_2SiS_5 and $Ce_4Si_3S_{12}$.* The X-ray powder diffraction diagrams of these two phases were recorded on a CPS120 INEL X-ray powder diffractometer equipped with a Cu K−L_3 monochromatized radiation (1.540598 Å) and a position-sensitive detector calibrated with $Na_2Ca_3Al_{12}F_{14}$ as standard (monochromator Cu K−L_3 radiation was selected with an asymmetric focusing incident-beam curved quartz monochromator). Powder samples were sieved at 20 μm and introduced in a Lindeman capillary (0.1-mm diam.). The structures of Ce_2SiS_5 and $Ce_4Si_3S_{12}$ had not been refined prior to the present study, although the cell parameters were determined from X-ray powder diffraction diagrams[17,18] starting from single-crystal studies carried out on analogous phases La_2GeS_5[19] and $La_4Ge_3S_{12}$.[20] On the basis of the structural arrangement of the two thiogermanates, the cell parameters and the atomic positions of Ce_2SiS_5 and $Ce_4Si_3S_{12}$ were successfully refined with the Rietveld method, using the Jana2000 program.[21] This confirmed the symmetry, space group, and cell parameters reported for the two phases. With only one rather weak diffraction line excluded for Ce_2SiS_5, a good purity of the samples at the X-ray detection threshold could be inferred. This is important for the validity of the optical studies (see below). Because of the high diffraction power of cerium, the atomic displacement parameters of light atoms had to be constrained to a unique refined parameter. Tables 1−4 summarize the recording conditions and the refinement results along with the atomic positions. Figures 1 and 2 give the observed and calculated diagrams along with the difference curves, which are quite satisfactory.

Single Crystal Study of $Ce_6Si_4S_{17}$. A single crystal of $Ce_6Si_4S_{17}$ was isolated from the preparation batch and analyzed by means of a Weissenberg camera. The diffraction intensities were then collected on a IPDS Stoe diffractometer in a medium resolution mode (imaging plate at 60 mm, limiting $\sin(\theta)/\lambda$ to 0.66 Å^{-1}). The Bragg vectors could be indexed according to a triclinic cell, leaving P1 and P$\bar{1}$ as possible space groups. After

Table 1. Structural Data and Crystallographic Data Recording/Refinement Conditions for Ce_2SiS_5

molecular weight (g·mol^{-1})	468.63
crystal symmetry	monoclinic
space group	P 2_1/c (14)
cell parameters	$a = 7.5475(8)$ Å
	$b = 12.5581(14)$ Å
	$c = 7.8286(8)$ Å
	$\beta = 101.550(3)°$
Z, V (Å^3)	4, 727.0(2)
λ (Å)	1.540598
d_{calc} (g·cm^{-3})	4.280
2θ range, $\Delta 2\theta$ steps	7.95−114.00°; 0.03°
number of reflections	984
number of refined parameters	74
excluded zone	51.2−51.4°
profile (pseudo Voigt)	4 parameters
asymmetry (Simpson)	1 parameter
background (Chebyshev polynoms)	36 parameters
absorption correction (Debye-Scherer/cylinder)	introduced but fixed
sample displacement	1 parameter

$R_p = 4.27\%$ $R_{wp} = 5.47\%$ $R_{Bragg} = 5.26\%$ $\chi^2 = 1.65$

Table 2. Atomic Positions and Isotropic Displacement Parameters[a] of Ce_2SiS_5

atom	x	y	z	U_{iso} (Å^2)
Ce(1)	0.2387(8)	0.4050(5)	0.5463(8)	0.016(3)
Ce(2)	0.8356(8)	0.1660(4)	0.3659(8)	0.015(3)
Si	0.322(3)	0.114(2)	0.596(3)	0.012(3)
S(1)	0.168(3)	0.031(2)	0.384(3)	0.012
S(2)	0.865(3)	0.378(2)	0.501(3)	0.012
S(3)	0.415(3)	0.003(2)	0.775(3)	0.012
S(4)	0.125(3)	0.2053(17)	0.691(3)	0.012
S(5)	0.522(3)	0.2281(18)	0.549(3)	0.012

[a] U_{iso} of light atoms (Si and S) have been constrained to the same refined value.

(17) Michelet, A.; Perez, G.; Etienne, J.; Darriet-Duale, M. *C. R. Acad. Sci. Paris C* **1970**, *271*, 513.
(18) Perez, G.; Duale, M. *C. R. Acad. Sci. Paris C* **1969**, *269*, 984.
(19) Mazurier, A.; Etienne, J. *Acta Crystallogr. B* **1973**, *29*, 817.
(20) Mazurier, A.; Etienne, J. *Acta Crystallogr. B* **1974**, *30*, 759.
(21) Petricek, V.; Dusek, M. *JANA2000*: Programs for Modulated and Composite Crystals; Institute of Physics: Praha, Czech Republic, 1998.

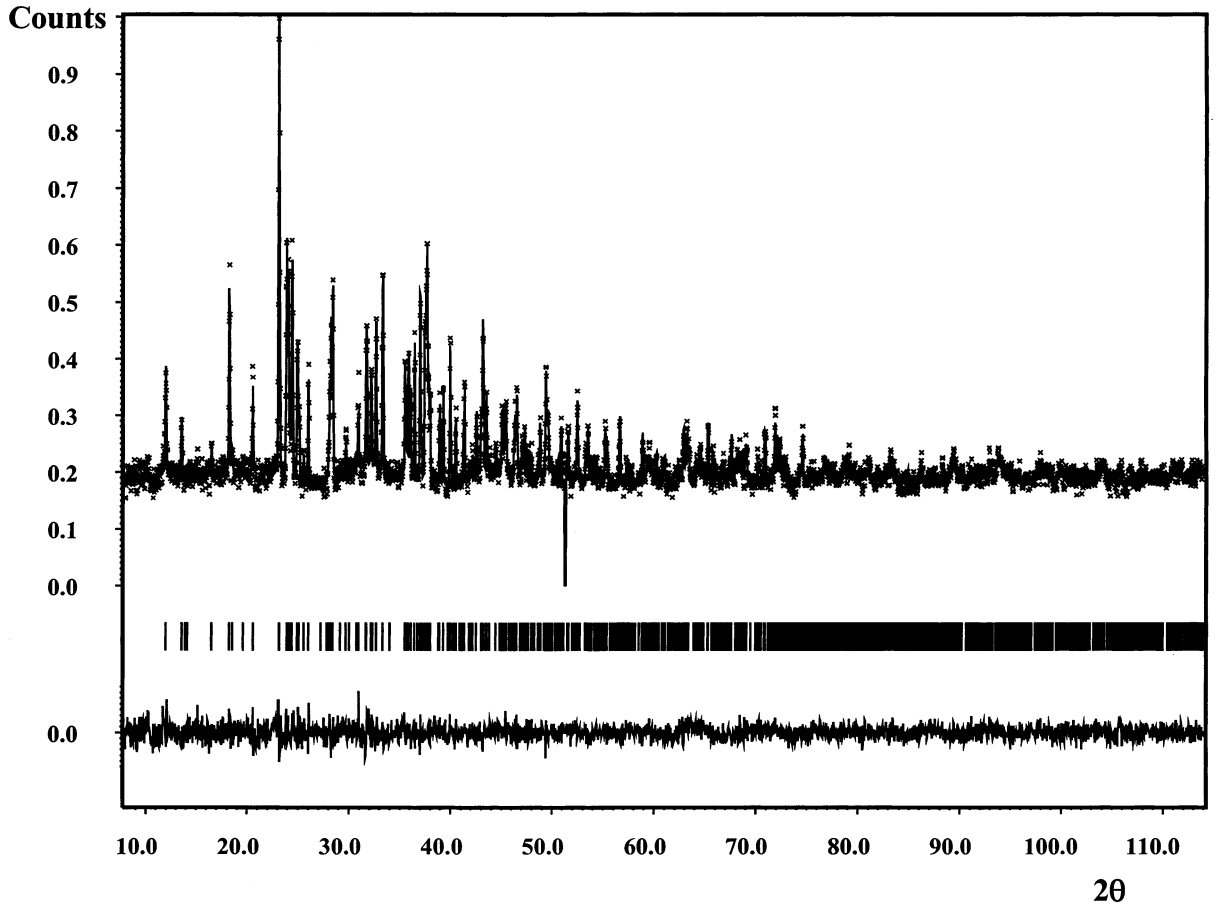

Figure 1. Calculated and observed powder X-ray diffraction patterns of Ce_2SiS_5. The difference diagram indicates a satisfactory structure refinement.

Table 3. Structural Data and Crystallographic Data Recording/Refinement Conditions for $Ce_4Si_3S_{12}$

molecular weight ($g \cdot mol^{-1}$)	1029.46
crystal symmetry	trigonal
space group	R 3c (161)
cell parameters	$a = 19.1745(5)$ Å
	$c = 7.9943(2)$ Å
Z, V (Å^3)	6, 2545.40(12)
λ (Å)	1.540598
d_{calc} ($g.cm^{-3}$)	4.028
2θ range, $\Delta 2\theta$ steps	12.45−93.99°; 0.03°
number of reflections	506
number of refined parameters	52
profile (pseudo Voigt)	4 parameters
asymmetry (Simpson)	1 parameter
background (Chebyshev polynoms)	22 parameters
absorption correction (Debye-Scherer/cylinder)	introduced but fixed
sample displacement	1 parameter

$R_p = 2.98\%$ $R_{wp} = 3.93\%$ $R_{Bragg} = 3.03\%$ $\chi^2 = 2.01$

Table 4. Atomic Positions and Isotropic Displacement Parameters[a] of $Ce_4Si_3S_{12}$

atom	x	y	z	U_{iso} (Å^2)
Ce(1)	0	0	0	0.010(2)
Ce(2)	0.2284(2)	0.2307(2)	0.7032(9)	0.0171(11)
Si	0.2010(11)	0.1864(9)	0.153(2)	0.011(2)
S(1)	0.2861(10)	0.1794(10)	−0.002(2)	0.011
S(2)	0.1258(8)	0.0675(10)	0.247(2)	0.011
S(3)	0.1178(10)	0.2019(10)	0.006(2)	0.011
S(4)	0.2677(9)	0.2684(9)	0.344(2)	0.011

[a] U_{iso} of light atoms (Si and S) have been constrained to the same refined value.

the usual correction (Lorentz-polarization with the Stoe program package [22] and absorption through a Gaussian integration process), the structure was partially solved in the $P\bar{1}$ space group, using the SHELXTL direct methods.[23] All subsequent calculations were carried out with the Jana2000 program.[21] The incomplete atomic arrangement was extended through a series of difference Fourier syntheses. With isotropic displacement parameters the residual factor converged to $R = 0.0523$ (Rw = 0.107). Introducing anisotropic displacement parameters and a secondary extinction coefficient,[24] it further reduced to the final value $R = 0.0426$ (Rw = 8.48). Recording and refinement conditions are summarized in Table 5. The atomic positions and equivalent displacement parameters are listed in Table 6.

(22) Stoe software. Stoe & Cie Gmbh: Darmstadt, Germany, 1996.
(23) Sheldrick, G. M. SHELXTL V5.0; Analytical X-ray Instruments Inc.: Madison, WI, 1995.
(24) Becker, P. J.; Coppens, P. *Acta Crystallogr. A* **1974**, *30*, 129.

3. Ce^{3+} Ion Environments

In understanding the optical properties of the cerium thiosilicates Ce_2SiS_5, $Ce_4Si_3S_{12}$, and $Ce_6Si_4S_{17}$ (see Section 4), it is essential to examine first the local environment of their Ce^{3+} ions in some detail. In this section, we show that $Ce_6Si_4S_{17}$ is distinguished from Ce_2SiS_5 and $Ce_4Si_3S_{12}$ in terms of their Ce^{3+} ion environments.

The structure of Ce_2SiS_5, isostructural to La_2GeS_5,[19] shows two different Ce sites, i.e., the 8-coordinate (bicapped trigonal prism) Ce(1) site and the 9-coordinate (tricapped trigonal prism) Ce(2) site. The [Ce(1)S_8] and [Ce(2)S_9] polyhedra share triangular faces, edges, and apex to form a three-dimensional lattice in which Si atoms occupy the tetrahedral sites to form [SiS_4] tetrahedral units. The average Ce−S distances of the

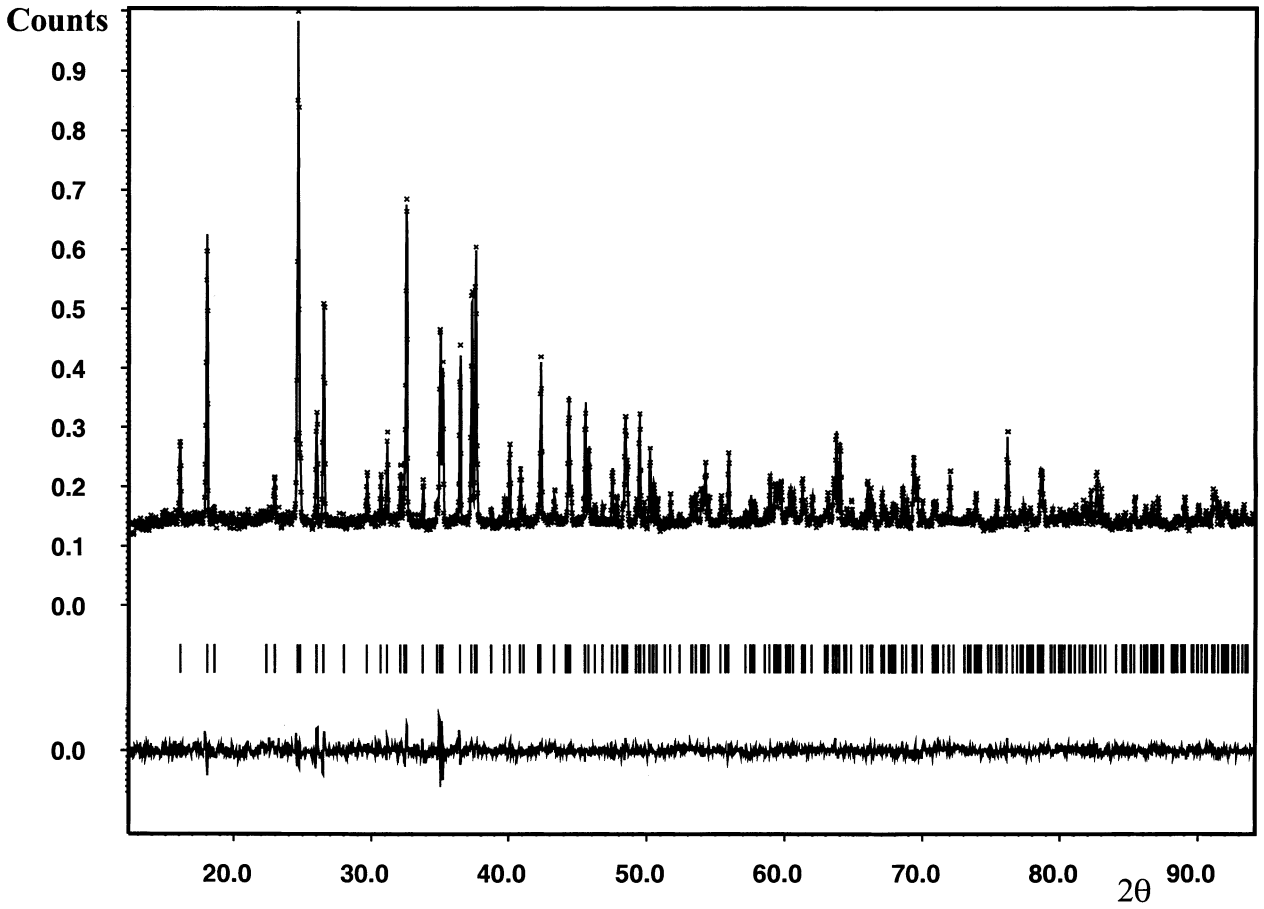

Figure 2. Calculated and observed powder X-ray diffraction patterns of $Ce_4Si_3S_{12}$. The difference diagram indicates a satisfactory structure refinement.

[Ce(1)S_8] and [Ce(2)S_9] units are 2.95 and 3.07 Å, respectively, which are in good agreement with those generally observed in similar environments of Ce^{3+} ions. For example, the Ce−S distances are 2.916(1)−3.065(1) Å in $CePS_4$,[12] and 2.901(2)−3.092(2) Å in γ-Ce_2S_3,[25] which have 8-coordinate Ce^{3+} ions. The Ce−S distances are 2.884(2)−3.346(2) Å in $K_3CeP_2S_8$[15] that has 9-coordinate Ce^{3+} ions. The mean Si−S distance and the mean S−Si−S angle within the SiS_4 tetrahedra are 2.12 Å and 109°, respectively. These values are close to those found for $Na_4Si_4S_{10}$[26] (Si−S = 2.025−2.162 Å and S−Si−S = 108.07−111.51°). The structural features of Ce_2SiS_5 are in agreement with the charge balance $(Ce^{3+})_2(Si^{4+})(S^{2-})_5$.

$Ce_4Si_3S_{12}$ is isostructural with $La_4Ge_3S_{12}$[20] and has two different Ce environments, i.e., tri-capped prisms [Ce(1)S_9] and bi-capped prisms [Ce(2)S_8]. Their mean Ce−S distances (3.05 and 3.02 Å, respectively) are also in good agreement with the expected ones. The Si atoms form SiS_4 tetrahedra with mean Si−S distance of 2.10 Å and mean S−Si−S angle of 109°. The structural features of $Ce_4Si_3S_{12}$ correspond to the charge balance $(Ce^{3+})_4(Si^{4+})_3(S^{2-})_{12}$.

$Ce_6Si_4S_{17}$ exhibits a new structure type. This compound contains six distinct Ce sites, namely, two tri-capped prisms ([Ce(1)S_9] and [Ce(2)S_9]), three bi-capped prisms ([Ce(3)S_8], [Ce(5)S_8], and [Ce(6)S_8)]), and one mono-capped prism ([Ce(4)S_7]). Considering only the Ce/S network, the structure can be described in terms of $^2/_\infty$[Ce_6S_{29}] layers running in the (011) plane in which the [CeS_9], [CeS_8], and [CeS_7] polyhedra are linked to each other via face-, edge-, and corner-sharing (Figure 3a). These layers condense by edge- and corner-sharing to form the $^3/_\infty$[Ce_6S_{17}] framework (Figure 3b). The [SiS_4] groups introduced between the layers strengthen the bonding between them, hence leading to the three-dimensional structure of $Ce_6Si_4S_{17}$ (Figure 3c). The average Ce−S distances (3.052 and 3.069 Å for the CeS_9 units; 2.996, 2.998, and 3.004 Å for the CeS_8 units; and 2.937 Å for the CeS_7 unit) are in agreement with the typical Ce^{3+}−S distances. (For the Ce−S distances of CeS_9 and CeS_8 units, see above. Those of a [CeS_7] unit are found in $KCeSiS_4$.[27]) Thus, the mean Ce−S distance becomes longer as the coordination number of Ce increases. As expected, the Si atoms are in tetrahedral sites with Si−S = 2.11−2.13 Å and the mean S−Si−S = 109.4°. The charge balance of the phase is written as $(Ce^{3+})_6(Si^{4+})_4(S^{2-})_{17}$.

For each unique Ce^{3+} site, Table 7 summarizes the coordination number, the Ce−S distances (minimum, maximum, and mean), the number of [SiS_4] tetrahedra surrounding the cerium polyhedra $[CeS_n]^{(2n-3)-}$ (n = 7−9), and the way the [SiS_4] tetrahedra are coordinated to the cerium polyhedra. The average coordination numbers of Ce are 8.5 in Ce_2SiS_5, 8.3 in $Ce_4Si_3S_{12}$, and

(25) Mauricot, R.; Evain, M.; Gressier, P.; Brec, R. *J. Alloys Compd.* **1995**, *223*, 130.

(26) Cade, A.; Ribes, M.; Philippot, E.; Maurin, M. *C. R. Acad. Sci. Paris C* **1972**, *274*, 1054.

(27) Gauthier, G.; Guillen, F.; Jobic, S.; Deniard, P.; Macaudière, P.; Fouassier, C.; Brec, R. *C. R. Acad. Sci. Paris* **1999**, 611.

Table 5. Structural Data and Crystallographic Data Recording/Refinement Conditions for $Ce_6Si_4S_{17}$

molecular weight ($g \cdot mol^{-1}$)	1498.08
crystal symmetry	triclinic
space group	P −1 (2)
cell parameters	$a = 8.9576(6)$ Å
(from powder at $T = 300K$)	$b = 10.0022(7)$ Å
	$c = 14.2651(10)$ Å
	$\alpha = 82.188(3)°$
	$\beta = 86.889(7)°$
	$\gamma = 89.515(4)°$
Z, V (Å^3)	2, 1264.4(2)
λ (Å)	0.71069
d_{calc} ($g \cdot cm^{-3}$)	3.934
diffractometer	STOE imaging plate diffraction system
φ-range, $\Delta(\varphi)$ step	0−250°; 1°
exposure time (min), completeness	8, 95%
2θ(°) angle domain (°)	3.8−56.3
recording range	$-10 \le h \le 10$, $-13 \le k \le 13$, $-18 \le l \le 18$
linear absorption coefficient	$\mu(\lambda_{MoK-L2,3}) = 121.6$ cm^{-1}
absorption correction	analytical Gaussian integration ($T_{min} = 0.179$; $T_{max} = 0.218$)
number of recorded reflections	15203
number of observed reflections ($I > 3\sigma(I)$)	4403
redundancy, Rint(%)	2.7, 8.05
number of independent reflections ($I > 3\sigma(I)$)	2215
refinement	F^2
F_{000}	1352
weighting scheme	$w = 1/(\sigma^2\|F_0\|+(0.016\|F_0\|)^2)$
number of refined parameters	245
residual factors	R(%) = 4.26, Rw(%) = 8.48, gof = 0.94
secondary extinction coefficient	0.015(4)
residual electronic density	[−2.9, +3.7] e$_-$/Å^3

Table 6. Atomic Positions and Displacement Parameters in $Ce_6Si_4S_{17}$

atom	x	y	z	U_{eq} (Å^2)
Ce(1)	0.47753(13)	0.73133(9)	0.54087(7)	0.0103(3)
Ce(2)	0.58162(13)	0.57886(9)	0.16660(7)	0.0092(3)
Ce(3)	0.83025(13)	0.91349(9)	0.34206(7)	0.0114(3)
Ce(4)	0.12796(14)	0.43096(10)	0.32673(8)	0.0137(3)
Ce(5)	0.39393(13)	0.11542(9)	0.18165(7)	0.0097(3)
Ce(6)	0.94665(12)	0.23952(9)	0.00062(7)	0.0088(3)
Si(1)	0.2500(6)	0.0000(4)	0.4154(3)	0.0112(16)
Si(2)	0.2487(6)	0.4410(4)	0.0773(3)	0.0115(16)
Si(3)	0.7311(6)	0.9382(4)	0.0987(3)	0.0106(15)
Si(4)	0.7735(6)	0.5567(4)	0.3949(3)	0.0101(15)
S(1)	0.8407(5)	0.5015(4)	0.0567(3)	0.0108(14)
S(2)	0.4863(5)	0.0036(4)	0.3771(3)	0.0121(14)
S(3)	0.3159(5)	0.5179(4)	0.4673(3)	0.0117(14)
S(4)	0.6059(5)	0.7000(4)	0.3460(3)	0.0101(14)
S(5)	0.1785(5)	0.0192(4)	0.0428(3)	0.0110(14)
S(6)	0.7972(6)	0.4107(4)	0.3047(3)	0.0147(15)
S(7)	0.5097(5)	0.8719(4)	0.1133(3)	0.0140(15)
S(8)	0.2415(5)	0.6149(3)	0.1498(3)	0.0105(14)
S(9)	0.4578(5)	0.3527(4)	0.0476(3)	0.0136(15)
S(10)	0.1145(5)	0.2886(4)	0.1605(3)	0.0102(14)
S(11)	0.4282(5)	0.3547(4)	0.2790(3)	0.0125(14)
S(12)	0.2054(5)	0.1905(4)	0.4598(3)	0.0131(14)
S(13)	0.1883(5)	0.8649(4)	0.5373(3)	0.0114(14)
S(14)	0.8674(5)	0.7844(4)	0.1666(3)	0.0120(14)
S(15)	0.1445(6)	−0.0297(4)	0.2926(3)	0.0197(16)
S(16)	0.7477(5)	0.1134(4)	0.1681(3)	0.0122(14)
S(17)	0.9818(5)	0.6520(4)	0.3981(3)	0.0152(15)

8.2 in $Ce_6Si_4S_{17}$ (Table 8). As already pointed out, the general formulas of the Ce−S−Si phases can be rewritten as $(Ce_2S_3)_m(SiS_2)_n$. Thus, the extent of SiS_2 per Ce_2S_3 increases in the order Ce_2SiS_5 ($^n/_m = 1$) < $Ce_6Si_4S_{17}$ ($^n/_m = {}^4/_3$) < $Ce_4Si_3S_{12}$ ($^n/_m = {}^3/_2$). A given SiS_4 tetrahedral unit coordinates to a Ce^{3+} ion with a corner or an

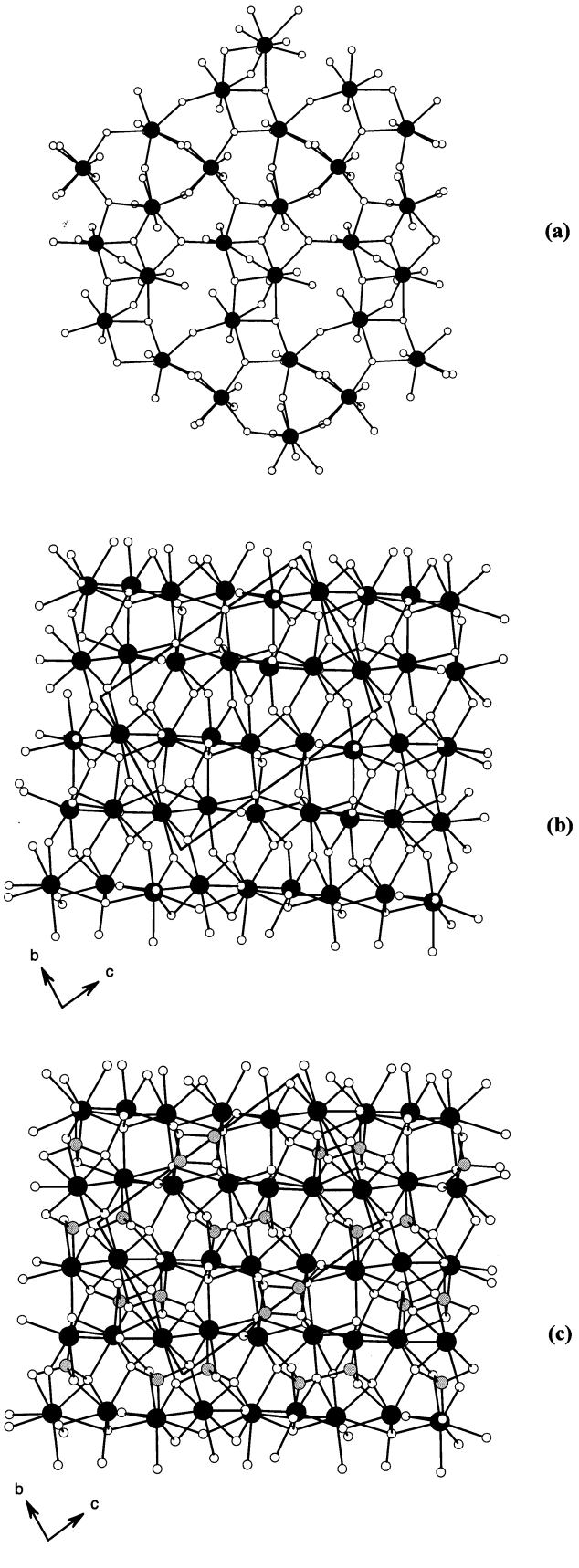

Figure 3. Description of the structure of $Ce_6Si_4S_{17}$: (a) $^2/_\infty[Ce_6S_{29}]$ layers running in the (011) plane; (b) $^3/_\infty[Ce_6S_{17}]$ framework built upon $^2/_\infty[Ce_6S_{29}]$ layers; (c) the three-dimensional structure of $Ce_6Si_4S_{17}$ with $[SiS_4]$ tetrahedra between $^2/_\infty[Ce_6S_{29}]$ layers (black, gray, and open circles represent Ce, Si, and S, respectively).

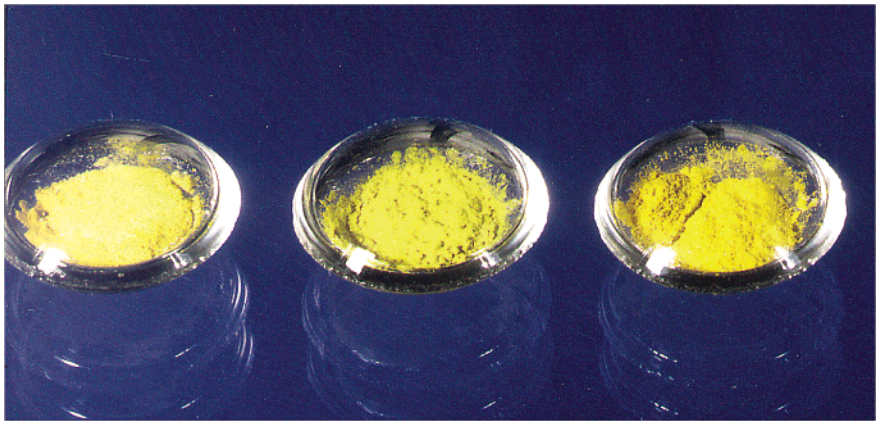

(a) **(b)** **(c)**

Figure 4. Colors of (a) $CePS_4$, (b) $Ce_6Si_4S_{17}$, and (c) $Ce_4Si_3S_{12}$.

edge. A "corner-coordination" generates one Ce−S−Si bond linkage, and an "edge-coordination" generates two Ce−S−Si bond linkages. Thus, from the Ce atom environments summarized in Table 7, it can be readily shown that the average number of Ce−S−Si bond linkages per Ce^{3+} ion increases with the increasing extent of SiS_2 per Ce_2S_3. In average, each Ce^{3+} ion is dominated by the contribution of the "edge-coordination" in $Ce_6Si_4S_{17}$, whereas the "corner-coordination" contributes slightly more than does the "edge-coordination" in Ce_2SiS_5 and $Ce_4Si_3S_{12}$ (Table 8). Thus, $Ce_6Si_4S_{17}$ is distinguished from Ce_2SiS_5 and $Ce_4Si_3S_{12}$ in terms of the mean coordination number of Ce^{3+}, and also in terms of the mean relative contribution of the SiS_4 "edge-coordination" around Ce^{3+}.

4. Optical Properties

The colors of $Ce_4Si_3S_{12}$ and $Ce_6Si_4S_{17}$ are presented in the photograph of Figure 4, where that of $CePS_4$, a good potential pigment, is added for comparison. Whereas $Ce_4Si_3S_{12}$ presents a golden color, $Ce_6Si_4S_{17}$ looks more like $CePS_4$ with a bright yellow hue. The color of Ce_2SiS_5 (not shown) resembles that of $Ce_4Si_3S_{12}$, but with a lesser brightness. Table 9 summarizes the L/a/b chromatic coefficients for the three Ce−S−Si phases determined from room temperature diffuse reflectance measurements of finely ground samples with a Perkin-Elmer Lambda II spectrometer ($BaSO_4$ powder was used as the reference for 100% reflectance). These coefficients confirm the visual observations. $Ce_4Si_3S_{12}$ and $Ce_6Si_4S_{17}$, with a high brightness (large L), a high purity (large Cab), and a hue angle h_{ab} close to the 90° expected for an ideal yellow color, appear as good candidates for yellow pigments (see below for their chemical and temperature stability). In contrast, Ce_2SiS_5 exhibits low L and Cab values indicating, as perceived, a lack of brightness and purity, in agreement with a somewhat somber color of the compound. As seen from the values of h_{ab} (equal to 85.13°), the yellow-gold color of $Ce_4Si_3S_{12}$ is very similar to that of Ce_2SiS_5. This agrees well with the diffuse reflectance spectrum of $Ce_4Si_3S_{12}$ (see below), which shows that the absorption onset is very close in energy to that found for Ce_2SiS_5.

The yellow color of $Ce_6Si_4S_{17}$ contains a green component (negative a value). The L, a, and b coefficients of $Ce_6Si_4S_{17}$ are quite close to those of $CePS_4$. The brightness is enhanced by a luminescence, covering the

Table 7. Structural Data for the Ce Atoms of Ce_2SiS_5, $Ce_4Si_3S_{12}$, and $Ce_6Si_4S_{17}$

Ce atom	CN	Ce−S distances (Å)	number of SiS_4 groups coordinated to the $[CeS_x]$ polydra and coordination mode
		compound: Ce_2SiS_5	
Ce(1)	8	mean: 2.95 min: 2.79(2) max: 3.08(2)	4 SiS_4 (2 edges + 2 corners) 2 S atoms unshared with Si
Ce(2)	9	mean: 3.07 min: 2.86(2) max: 3.34(2)	5 SiS_4 (2 edges + 3 corners) 2 S atoms unshared with Si
		compound: $Ce_4Si_3S_{12}$	
Ce(1)	9	mean: 3.05 min: 2.87(2) max: 3.37(2)	6 SiS_4 (3 edges + 3 corners)
Ce(2)	8	mean: 3.02 min: 2.85(2) max: 3.49(2)	6 SiS_4 (2 edges + 4 corners)
		compound: $Ce_6Si_4S_{17}$	
Ce(1)	9	mean: 3.052 min: 2.771(4) max: 3.398(5)	4 SiS_4 (4 edges + 0 corner) 1 S atom unshared with Si
Ce(2)	9	mean: 3.069 min: 2.885(4) max: 3.297(4)	4 SiS_4 (4 edges + 0 corner) 1 S atom unshared with Si
Ce(3)	8	mean: 2.996 min: 2.878(4) max: 3.234(5)	5 SiS_4 (3 edges + 2 corners)
Ce(4)	7	mean: 2.937 min: 2.839(4) max: 3.046(4)	4 SiS_4 (2 edges + 2 corners) 1 S atom unshared with Si
Ce(5)	8	mean: 2.998 min: 2.878(4) max: 3.165(5)	4 SiS_4 (3 edges + 1 corner) 1 S atom unshared with Si
Ce(6)	8	mean: 3.004 min: 2.870(4) max: 3.216(4)	4 SiS_4 (4 edges + 0 corner)

Table 8. Comparison of the Observed Ce^{3+} 4f→5d Gaps with the Mean Coordination Number of Ce and the Mean Contribution of the Edge-Sharing SiS_4 Tetrahedra around Ce

sample	CN of Ce	contribution of edge-sharing SiS_4*	E_g (eV)
Ce_2SiS_5	8.5	44%	2.34(1)
$Ce_4Si_3S_{12}$	8.3	38%	2.38(1)
$Ce_6Si_4S_{17}$	8.2	80%	2.56(1)

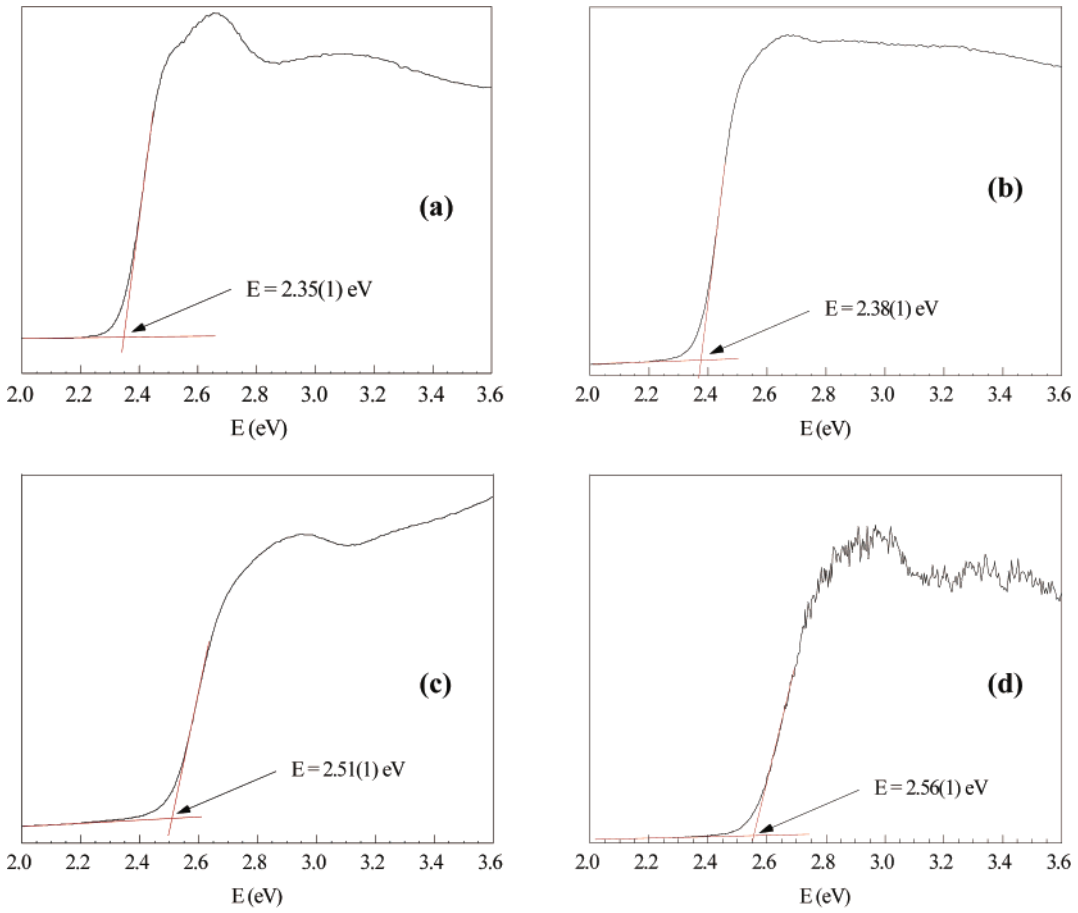

Figure 5. Diffuse reflection spectra (Kubelka−Munk transformed) of the Ce−S−Si phases at room temperature (K/S vs E): (a) Ce_2SiS_5, (b) $Ce_4Si_3S_{12}$, (c) $Ce_6Si_4S_{17}$ recorded without background monochromator, and (d) $Ce_6Si_4S_{17}$ recorded with background monochromator.

Table 9. Chromatic Coefficients of Ce_2SiS_5, $Ce_6Si_4S_{17}$, $Ce_4Si_3S_{12}$, $CePS_4$, and Some Inorganic Yellow Commercial Pigments

phase	L[a]	a	b	C_{ab}	h_{ab}	$d = \lvert h_{ab} - 90° \rvert$
Ce_2SiS_5	56.46	4.16	48.81	48.99	85.13	4.87
$Ce_6Si_4S_{17}$	81.63	−10.00	68.25	68.98	98.34	8.34
$Ce_4Si_3S_{12}$	73.95	6.75	75.45	75.75	84.89	5.11
$CePS_4$	85.97	−9.45	75.73	76.32	97.11	7.11
$PbCrO_4$	87.9	3.8	98.40	98.47	87.79	2.21
$BiVO_4$	90.4	−8.7	86.10	86.54	95.77	4.23
$NiTiO_3$	89.2	−9.6	54.40	55.24	100.01	10.01
CdS	90.4	−6.0	95.10	95.29	93.61	3.61

[a] L axis: white(100)/black(0). a axis: red(+)/green(−). b axis: yellow(+)/blue(−). $C_{ab} = \sqrt{a^2+b^2}$: purity of hue (0−100). h_{ab} = arctan(b/a): angle of hue (yellow = 90°).

green and yellow, easily detected under UV lighting (see below).

The diffuse reflectance spectra (Kubelka−Munk transformed) of Ce_2SiS_5, $Ce_4Si_3S_{12}$, and $Ce_6Si_4S_{17}$ are presented in Figure 5. For Ce_2SiS_5 and $Ce_4Si_3S_{12}$ the absorption edges lie at 2.35(1) eV and 2.38(1) eV, respectively. The steep absorption at higher energy is attributable to the lowest-energy Ce^{3+} 4f→5d transition. It is interesting to consider the shapes of the absorption spectra (Figure 5) around the absorption thresholds. Ce_2SiS_5 has a shape suggestive of two overlapping absorption bands. This feature is weakened in the spectra of $Ce_4Si_3S_{12}$ and $Ce_6Si_4S_{17}$.

The absorption spectra of the luminescent $Ce_6Si_4S_{17}$ material were recorded without and with a monochromator between the sample and the detector (using the Perkin-Elmer Lambda spectrometer and a Spex Fluorolog FL212 spectrofluorometer, respectively) (Figure 5c,d). Because the luminescence efficiency is low, the reflectance spectrum in Figure 5c is hardly modified by the emitted light. The absorption threshold derived from Figure 5d lies at 2.56(1) eV.

5. Gap of the Ce^{3+} 4f→5d Transition

As already discussed, $Ce_6Si_4S_{17}$ differs from Ce_2SiS_5 and $Ce_4Si_3S_{12}$ in terms of the Ce^{3+}-ion environments. The same is also true in terms of the observed Ce^{3+} 4f→5d gaps: E_g is 2.56 eV for $Ce_6Si_4S_{17}$, and ∼2.36 eV for Ce_2SiS_5 and $Ce_4Si_3S_{12}$ (Table 8). The 4f→5d gaps of the three compounds do not correlate with their Ce/Si ratios. To probe what structural/electronic factors determine the 4f→5d absorption gap, we carried out electronic structure calculations for the three Ce−S−Si phases using the extended Hückel method.[28,29] The parameters of the atomic orbitals employed in our calculations are listed in Table 10. The 4f levels of the Ce atoms in the Ce−S−Si phases lie below the bottom of their conduction bands made up of the Ce 5d and the S 3s/3p orbitals, so that a Ce^{3+} cation with higher net positive charge will have a lower-lying 4f level and hence

(28) Whangbo, M.-H.; Hoffmann, R. *J. Am. Chem. Soc.* **1978**, *100*, 6093.
(29) Ren, J.; Liang, W.; Whangbo, M.-H. *CAESAR, Crystal and Electronic Structure Analyzer;* http://www.primec.com/, 1998.

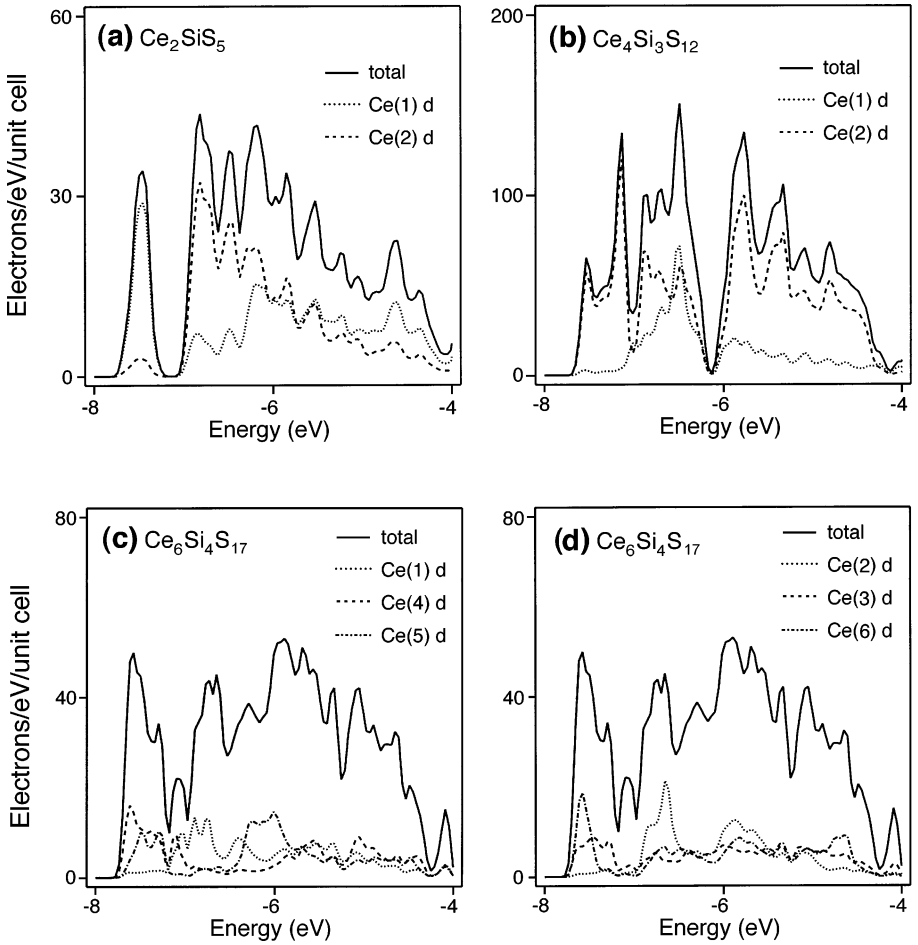

Figure 6. Total and partial density of state curves calculated for the conduction bands of (a) Ce_2SiS_5, (b) $Ce_4Si_3S_{12}$, and (c, d) $Ce_6Si_4S_{17}$.

Table 10. Exponents ζ_1 and Valence Shell Ionization Potentials H_{ii} of Slater-Type Orbitals χ_i Used for Extended Hückel Tight-Binding Calculation[a]

atom	χ_i	H_{ii} (eV)	ζ_1	c_1[b]	ζ_2	c_2[b]
Ce	6s	−7.67	2.140	1.0		
Ce	6p	−5.01	2.080	1.0		
Ce	5d	−8.21	3.780	0.7765	1.381	0.4586
Si	3s	−17.3	1.634	1.0		
Si	3p	−9.20	1.428	1.0		
S	3s	−20.0	2.122	1.0		
S	3p	−13.3	1.827	1.0		

[a] H_{ii}'s are the diagonal matrix elements $\langle\chi_i|H^{eff}|\chi_i\rangle$, where H^{eff} is the effective Hamiltonian. In our calculations of the off-diagonal matrix elements $H^{eff} = \langle\chi_i|H^{eff}|\chi_j\rangle$, the weighted formula was used. See: Ammeter, J.; Bürgi, H.-B.; Thibeault, J.; Hoffmann, R. *J. Am. Chem. Soc.* **1978**, *100*, 3686. [b] Coefficients used in the double-ζ Slater-type orbital expansion.

a larger 4f→5d absorption gap.[12] The 4f orbitals of Ce are not included in our calculations because the charges on Ce^{3+} ions are primarily determined by the interactions of the 5d obitals of Ce with the 3s/3p orbitals of the surrounding S ligands and because extended Hückel calculations do not include the effect of charge on the energy level. Our qualitative discussion will rely on the net positive charge of the Ce atoms obtained from the calculations. The trends in the results of our calculations do not depend on small variations in the atomic parameters. The objective of our calculations is to examine qualitatively why Ce^{3+} 4f→5d gap is wider for $Ce_6Si_4S_{17}$ than for Ce_2SiS_5 and $Ce_4Si_3S_{12}$. It is not our aim to reproduce the observed E_g values.

The density of states (DOS) plots calculated for the conduction bands of the three Ce−S−Si phases are presented in Figure 6. It is clear that the bottom position of the conduction bands changes little from one compound to another (−7.70, −7.64, and −7.70 eV for Ce_2SiS_5, $Ce_4Si_3S_{12}$, and $Ce_6Si_4S_{17}$, respectively). Namely, the bottom position of the conduction bands is not much influenced by the presence of different Ce sites in these compounds. However, the major Ce 5d orbital contributions to the bottom part of the conduction bands come from the Ce atom with the lowest coordination number in each Ce−S−Si phase. Hence, for Ce_2SiS_5 and $Ce_4Si_3S_{12}$, the lower part of the conduction bands is dominated by the 5d orbitals of the 8-coordinate Ce atoms. The 9-coordinate Ce atoms present more destabilized 5d-block levels. Qualitatively, this may be rationalized by noting that the d-block bands are antibonding between Ce and S, so a higher coordination leads to a stronger antibonding. This trend is also observed for $Ce_6Si_4S_{17}$, except that the contributions of the 7- and some 8-coordinate Ce atoms are similar (Figure 6c).

Because the conduction-band bottom is at about the same energy in the three Ce−S−Si phases, the differences in their Ce^{3+} 4f→5d gaps should originate mainly from the position of the 4f levels of their Ce atoms. As has been pointed earlier by Gauthier et al.,[12] the Ce 4f levels of a Ce^{3+} ion are lower in energy if the net positive charge on the Ce^{3+} ion is higher, thereby increasing the

Table 11. Calculated Net Positive Charges on the Ce Atoms of the Ce−Si−S Phases

compound	Ce/CN	Ce charge
Ce_2SiS_5	Ce(1)/8	+1.11
	Ce(2)/9	+1.29
$Ce_4Si_3S_{12}$	Ce(1)/9	+1.14
	Ce(2)/8	+1.22
$Ce_6Si_4S_{17}$	Ce(1)/9	+1.28
	Ce(2)/9	+1.29
	Ce(3)/8	+1.27
	Ce(4)/7	+1.26
	Ce(5)/8	+1.25
	Ce(6)/8	+1.29

Ce^{3+} 4f→5d gap. The net positive charges calculated for the Ce atoms of the three Ce−S−Si phases (Table 11) show that one of the two unique Ce atoms in both Ce_2SiS_5 and $Ce_4Si_3S_{12}$ has a significantly lower net charge (∼1.12 against ∼1.25), and that all the Ce atoms of $Ce_6Si_4S_{17}$ have a higher net positive charge than do those of Ce_2SiS_5 and $Ce_4Si_3S_{12}$. This accounts for why the Ce^{3+} 4f→5d gap is smaller in Ce_2SiS_5 and $Ce_4Si_3S_{12}$ than in $Ce_6Si_4S_{17}$. However, in reaching this conclusion, the propensity for Ce^{3+} cations to undergo an intrasite 4f→5d transition was not taken into consideration. In $Ce_4Si_3S_{12}$, the low net charge is found on the 9-coordinate Ce(1) atom. The 5d orbital contribution of Ce(1) to the conduction bands occurs mainly in the energy region well above the conduction band bottom (Figure 6b). Because the intersite 4f→5d transition is unlikely, the low energy absorption threshold observed for $Ce_4Si_3S_{12}$ must originate from the intrasite 4f→5d electronic transition of Ce(1). The latter is possible because the 5d orbital contribution of Ce(1) to the bottom of the conduction band is nonzero. Such a low contribution is indeed sufficient to make the transition possible, as demonstrated from XANES and EELS spectra simulations on several materials.[30] This reasoning suggests that in cerium thiosilicate materials the cerium with the lowest positive charge will determine the absorption threshold.

6. Luminescence of $Ce_6Si_4S_{17}$

At room temperature under UV light (λ_{exc} = 254 nm), $Ce_6Si_4S_{17}$ exhibits a green luminescence. The excitation (λ_{em} = 560 nm) and emission (λ_{exc}= 350 nm) spectra of $Ce_6Si_4S_{17}$ at 300 K are given in Figure 7. From the excitation spectrum, the highest luminescence intensity is obtained for direct excitation of Ce^{3+} at ∼2.75 eV. From the emission spectra, the radiative de-excitation is found to occur in the form of the double band $5d^1 \rightarrow {}^2F_{5/2}$ and $5d^1 \rightarrow {}^2F_{7/2}$, where the ${}^2F_{5/2}$ and ${}^2F_{7/2}$ states originate from the splitting of the $4f^1$ state by the spin−orbit coupling. The fitting of the emission spectrum by two Gaussian bands shows (see the inset) that the two components are separated by about 0.19 eV, and the highest-energy band is located at 2.43 eV (λ = 510 nm) in energy. In contrast to the emission spectra of diluted Ce^{3+} ions, the higher energy band, $5d^1 \rightarrow {}^2F_{5/2}$, has a lower intensity than does the lower energy band, $5d^1 \rightarrow {}^2F_{7/2}$. This is due to a reabsorption mechanism, as shown by the overlap of the excitation and emission spectra (Figure 7). Despite the presence of six different

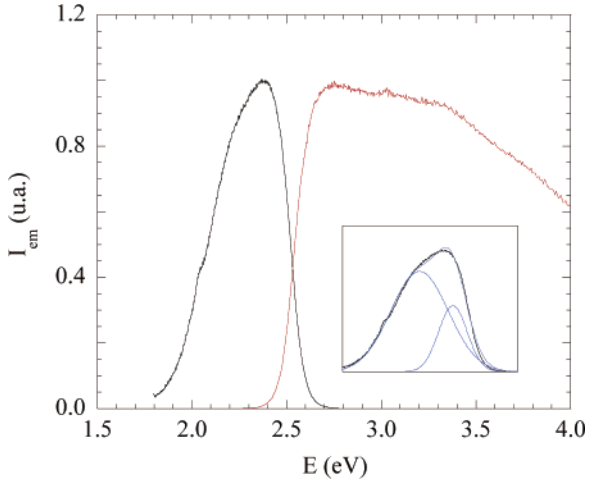

Figure 7. Emission (λ_{exc} = 350 nm) and excitation (λ_{em} = 560 nm) spectra of $Ce_6Si_4S_{17}$ (Inset: deconvolution of the emission spectrum).

Ce sites in the compound, the emission spectrum has a width and a shape hinting that at least at ambient temperature not all different Ce^{3+} sites are involved in the emission. This is usual at high cerium concentration, because, owing to the high probability of 4f→5d transitions, energy transfer between Ce^{3+} ions occurs at long distance so that only the Ce^{3+} ions with the lowest-energy absorption edge emit.

The excitation fluorescence spectrum (λ_{em} = 560 nm) is also shown in Figure 7. This spectrum is quite wide, in agreement with the splitting of the 5d-block levels of each Ce^{3+} ion. The Stokes shift at room-temperature calculated from the lower−energy band maximum is 0.32 eV (i.e., 2.43 vs. 2.75 eV). This value is slightly higher than those in sulfides such as MS and MGa_2S_4 (M = Ca, Sr)[31] or $KCeSiS_4$,[27] but is lower than those in the halothiosilicates $Ln_3(SiS_4)_2X$ (X = Cl, Br, I) (e.g., 0.57 eV in $La(SiS_4)_2I$).[32]

The quantum efficiency of $Ce_6Si_4S_{17}$ is low (η_{int} = 10%). The overlap of the emission and absorption spectra is too pronounced to avoid energy migration among Ce^{3+} ions up to defects. Low quenching materials such as $La_{1-x}Ce_xF_3$ and $La_{1-x}Ce_xMgAl_{11}O_{19}$ are characterized by much larger Stokes shifts (0.68 and 1.00 eV, respectively).[33,34] Another cause for nonradiative losses may be thermal quenching, although the 4f→5d emission of rare earth ions generally shows a high thermal stability.

The fact that $Ce_6Si_4S_{17}$ shows luminescence at room temperature, while Ce_2SiS_5 and $Ce_4Si_3S_{12}$ do not, implies concentration quenching, higher thermal stability, or both. The existence of six nonequivalent Ce sites is a favorable characteristic for limiting energy migration among Ce^{3+} ions. After energy transfer is made to the ions possessing the lowest 5d levels, energy transfer to ions possessing higher emitting levels is hindered by the absence of spectral overlap between the emission

(30) Wu, Z. Y.; Ouvrard, G.; Gressier, P.; Natoli, C. R. *Phys. Rev. B* **1997**, *55*, 10382.

(31) Ronot-Limousin, I.; Garcia, A.; Fouassier, C.; Barthou, C.; Benalloul, P.; Benoit, J. *J. Electrochem. Soc.* **1997**, *144*, 687.

(32) Riccardi, R.; Gout, D.; Gauthier, G.; Guillen, F.; Jobic, S.; Garcia, A.; Huguenin, D.; Macaudière, P.; Fouassier, C.; Brec, R. *J. Solid State Chem.* **1999**, *147*, 259.

(33) Elias, L. R.; Heaps, W. S.; Yen, W. M. *Phys. Rev.* **1973**, *8*, 4989.

(34) Verstegen, J. M.; Sommerdijk, J. L.; Verriet, J. G. *J. Lumin.* **1973**, *6*, 425.

of the former and the absorption of the latter. In the configuration coordinate model, the potential curves of the ground and first-excited electronic states are shifted by ΔR along the abscissa due to a change in the nature of occupied orbitals. The stability of the emission decreases with decreasing energy of the excited state and increasing ΔR. As already noted, the Ce sites of the Ce−S−Si phases have the highest mean relative contribution of SiS_4 edge-coordination in $Ce_6Si_4S_{17}$. This leads to a more rigid structural environment than does the corner-coordination. The preference for the edge-coordination in $Ce_6Si_4S_{17}$ would lead to a smaller ΔR compared with the case of Ce_2SiS_5 and $Ce_4Si_3S_{12}$.

7. Industrial Potential

As pointed out above, of the three Ce−S−Si phases under study, only $Ce_6Si_4S_{17}$ and $Ce_4Si_3S_{12}$ exhibit chromatic properties that are comparable to those of the industrial pigments (Table 9). To use these compounds in household plastic appliances such as dishes, it is necessary to determine their chemical/thermal stability. In the plastic moulds used for the fabrication of such utensils, the temperature may reach up to 300 °C. To examine the thermal stability, differential thermal analysis (DTA) and thermogravimetry analysis (TGA) were carried out for $Ce_6Si_4S_{17}$ and $Ce_4Si_3S_{12}$ (with masses of 67.2 mg and 76.6 mg, respectively) from room temperature up to 1000 °C, with a heating rate of 5°/min under an air flow of 1.3 L/hr. The DTA and TGA curves for both compounds show (Figure 8) a good thermal stability up to 500 °C, with a reaction starting above ~550 °C. After reaction, the two oxidized materials are white indicating a complete reaction with oxygen. This represents a significant improvement in thermal stability, compared with $CePS_4$ that reacts in air at about 350 °C. In addition, aqueous suspensions of $Ce_6Si_4S_{17}$ and $Ce_4Si_3S_{12}$ exhibit a reasonable stability because they show no apparent reaction after 8 h and a loss of color after 3 days. From all these experiments, it appears that these two compounds can probably be industrially processed into plastic matrix.

8. Concluding Remarks

On the basis of the inductive effect as a guiding principle, we examined cerium thiosilicates as potential yellow pigments. Our synthesis effort led to a new Ce−Si−S phase, $Ce_6Si_4S_{17}$, in addition to Ce_2SiS_5 and $Ce_4Si_3S_{12}$ reported previously. $Ce_6Si_4S_{17}$ is distinguished from Ce_2SiS_5 and $Ce_4Si_3S_{12}$ in terms of the mean coordination number of Ce, the mean contribution of edge-coordinate SiS_4 around Ce, luminescence at room temperature, and Ce^{3+} 4f→5d gap. Our electronic band structure calculations indicate that the Ce^{3+} 4f→5d gap is larger for $Ce_6Si_4S_{17}$ than for Ce_2SiS_5 and $Ce_4Si_3S_{12}$, because the last two compounds possess Ce atoms of lower net positive charge. Room-temperature luminescence occurs in $Ce_6Si_4S_{17}$, but not in Ce_2SiS_5 and $Ce_4Si_3S_{12}$, probably because the high number of crystallographic sites hinders Ce→Ce energy transfer processes responsible for concentration quenching. $Ce_6Si_4S_{17}$ and $Ce_4Si_3S_{12}$ possess color properties quite close to those of known inorganic commercial pigments; the brightness of the former is enhanced by its luminescence. Both exhibit high chemical and thermal stability. Thus these two compounds are potentially important yellow pigments worthy of large-scale industrial testing.

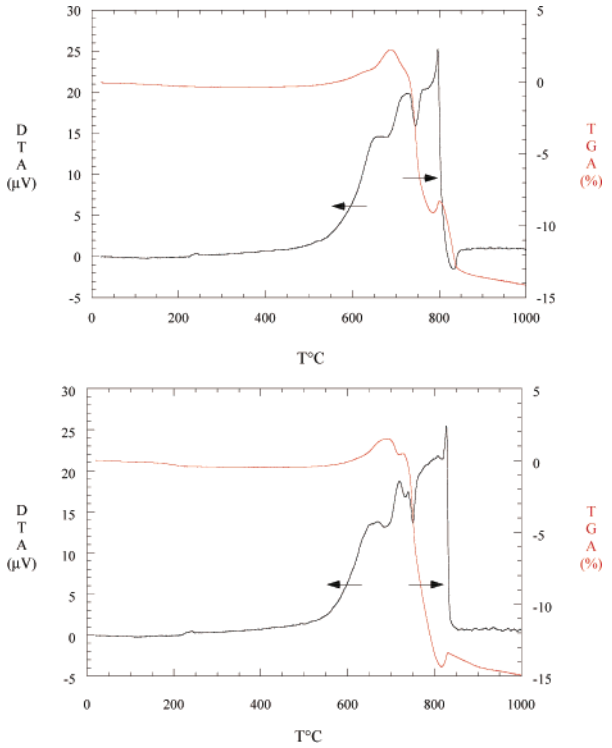

Figure 8. DTA and TGA curves under air flow: (a) $Ce_6Si_4S_{17}$ and (b) $Ce_4Si_3S_{12}$.

Acknowledgment. The work at North Carolina State University was supported by the Office of Basic Energy Sciences, Division of Materials Sciences, U.S. Department of Energy, under Grant DE-FG02-86ER45259. We are grateful to François Guillen for his help in optical measurements.

CM0211711